tvst

DOI: 10.1167/tvst.6.4.9

Article

Associations between Optic Nerve Head–Related Anatomical Parameters and Refractive Error over the Full Range of Glaucoma Severity

Neda Baniasadi[1,2], Mengyu Wang[1], Hui Wang[1,3], Mufeed Mahd[4], and Tobias Elze[1,5]

[1] Schepens Eye Research Institute, Harvard Medical School, Department of Ophthalmology, Boston, MA, USA
[2] University of Massachusetts, Department of Biomedical Engineering and Biotechnology, Lowell, MA, USA
[3] Institute for Psychology and Behavior, Jilin University of Finance and Economics, Department of Psychology, Changchun, Jilin, China
[4] University of Massachusetts, Department of Electrical and Computer Engineering, Lowell, MA, USA
[5] Max Planck Institute for Mathematics in the Sciences, Leipzig, Germany

Correspondence: Tobias Elze, Ph.D., Schepens Eye Research Institute Harvard Medical School 20 Staniford Street Boston, MA 02114, USA. e-mail: tobias_elze@meei.harvard.edu

Received: 9 February 2017
Accepted: 11 June 2017
Published: 18 July 2017

Keywords: optic nerve head; optical coherence tomography; spherical equivalent of refractive error; ametropia; glaucoma

Citation: Baniasadi N, Wang M, Wang H, Mahd M, Elze T. Associations between optic nerve head–related anatomical parameters and refractive error over the full range of glaucoma severity. Trans Vis Sci Tech. 2017;6(4):9, doi:10.1167/tvst.6.4.9

Purpose: To evaluate the associations between optic disc (OD)-related anatomical parameters (interartery angle [IAA] between superior and inferior temporal retinal arteries, OD tilt [TL], rotation [ROT], and torsion [TO], OD surface curvature [CUR], and central retinal vessel trunk entry point location [CRVTL] on OD) and the spherical equivalent of refractive error (SE), and to assess the impact of glaucoma severity on these relationships.

Methods: Cirrus optical coherence tomography (OCT) fundus images and 24-2 visual fields of 438 patients were included. Ellipses were fitted to OD borders. IAA was calculated between marked retinal artery locations on a circle around OD. Blood vessel entry point on OD was marked to locate CRVTL. TL was measured as the angle between the lines fitted to OD clinical boundary and the Bruch's membrane edges on the horizontal B-scans. Ellipse rotation relative to the vertical axis defined ROT. Angle between the long axis of OD and the interartery line defined TO. CUR was determined by the inner limiting membrane on the horizontal B-scans. Linear regression models evaluated by Bayes Factors (BF) were used to determine the covariance structure between the parameters and SE as well as possible impacts of mean deviation (MD).

Results: Our results showed that CRVTL had the strongest relationship with SE, followed by ROT, TL, and IAA (BFs: 3.59×10^7, 2645, 1126, and 248, respectively). MD did not significantly modulate the relationship between ONH parameters and SE.

Conclusion: Our results suggest that SE should be considered when interpreting the OD and its circumpapillary region for diagnostic purposes.

Translational Relevance: The reported relationships between OD-related parameters and ametropia may help to decrease false-positive clinical diagnoses of optic neuropathies.

Introduction

Myopia is a visual condition with a high prevalence[1–5] in which light focuses before instead of on the retina, resulting in a blurry perception of distant objects. Although myopia can also be caused by conditions related to the refractive elements of the eye, for instance diseases like nuclear cataract, in majority of the cases, myopia is caused by an elongation of the eye.[6–9] It has been shown that ocular axial length (AL) is strongly correlated with the refractive error, with each 1-mm increase in AL adding approximately 2 to 2.5 diopters (D) to refractive error.[10]

In addition to this well-documented connection between spherical equivalent (SE) of refractive error and eye elongation,[11,12] relationships between myopia and several parameters related to the optic nerve head (ONH) have been discussed.[13,14] However, previous studies[13,14] mainly focused on myopic patients and did not report their findings over the full range of SE.

As the appearance of the ONH is an important diagnostic criterion for optic neuropathies, particularly glaucoma,[15–17] a deeper insight into relationships between ONH parameters and SE may be clinically relevant.

Clinical eye examinations traditionally focus on the visual inspection of the fundus perpendicular to the retina, that is, the two-dimensional (2D) projection of the retina surface is inspected, and a number of ONH related parameters accessible in this 2D representation have been related to SE.[18–20] In recent years, technologies like optical coherence tomography (OCT) have been clinically applied to additionally image the retina in depth, which allows the definition of new parameters and their investigation in the context of ametropia. In this work, we combine traditional parameters defined in 2D with parameters that include OCT-derived depth information and study these relationships not only in myopic patients but also over the full range of SE.

The aim of this study was to investigate the relationships between the degree of ametropia, quantified by SE, and several anatomical parameters: (1) angle between major temporal superior and inferior retinal arteries (interartery angle, IAA); (2) ovality index (OI); (3) ONH vertical tilt (TL); (4) optic disc rotation (ROT); (5) optic disc torsion (TO); (6) location of the central retinal vessel trunk (CRVT) entry point on the optic disc (CRVTL); (7) ONH surface curvature (CUR), which are relevant for diagnostic purposes. In the first part, we quantify the relationship of these parameters with SE in a population of patients from a large clinical glaucoma practice and investigate their covariation structure by multivariate model comparisons. In the second part, we study whether glaucoma severity has an impact on these relationships.

Materials and Methods

This retrospective, cross-sectional study was approved by the institutional review board of Massachusetts Eye and Ear (MEE) and followed the tenets of the Declaration of Helsinki. We initially included the entire population of glaucoma patients and glaucoma suspects presented at MEE glaucoma service between 2011 and 2014.

Visual fields (VFs; protocol: SITA Standard 24-2; Humphrey Field Analyzer HFA-II, Carl Zeiss Meditec AG, Jena, Germany) and circumpapillary spectral-domain OCT measurements (protocol: Optic Disc Cube 200 × 200; Cirrus HD83 OCT, software version 6.5; Carl Zeiss Meditec AG, Jena, Germany) around the ONH within 1 year of the VF of all patients from MEE glaucoma service were collected.

For this study, the following reliability criteria were applied: VFs: false positive/negative rates $\leq 20\%$ and fixation loss rate $\leq 33\%$; OCT: signal strength ≥ 6, ONH center less than 3 mm in vertical or horizontal direction from image center, no missing data (black pixels on thickness plot) inside the standard scanning circle (radius of 1.73 mm around ONH), no motion artifacts detected by a trained observer (i.e., no vessel shifts of more than one vessel diameter or visible shifts within the optic disc).

Furthermore, the MEE medical records of the patients were checked for confounding diseases, and eyes with visually significant cataract (3+ nuclear sclerosis or worse), pseudophakia or aphakia, keratoconus, or macular degeneration, were excluded. Finally, all measurements were excluded for which no accompanying manifest SE of refractive error values were available. The SE was determined by subjective refraction.

Mean deviation (MD) was used as a measure of glaucoma severity.

ONH center and border were automatically determined by the Cirrus OCT software based on the three-dimensional volume scans. ONH center was defined as the gravity point of the ONH border, which, in turn, was defined by Bruch's membrane opening (BMO) identified on horizontal B-scans.[21] Ellipses were fitted to the ONH border with the ONH center as center and three free parameters (long axis, short axis, and rotation angle) by minimizing the mismatch between the area of the optic disc and the ellipse using the minimization algorithm from Nelder and Mead.[22] A trained observer marked the entry point for major blood vessels of retina on the short axis of this ellipse to locate CRVTL, and the intersections of the main superior temporal and inferior temporal arteries (STa and ITa) with the Cirrus standard measurement circle surrounding ONH (radius: 1.73 mm) to determine the IAA (Fig. 1A). Interartery line is the line that divides IAA into a superior and an inferior temporal sector (Fig. 1B). We developed a custom software in the programming language R (version 3.1.1; R Foundation, Vienna, Austria) for vessel tracking. All eyes were represented in right-eye orientation. CRVTL was normalized between 0 (temporal pole of ONH) and 1 (nasal pole of ONH).

ONH rotation (ROT) was measured as the angle between the main axis of the ellipse and the vertical reference line,[13,23,24] Unlike ROT, ONH torsion (TO)

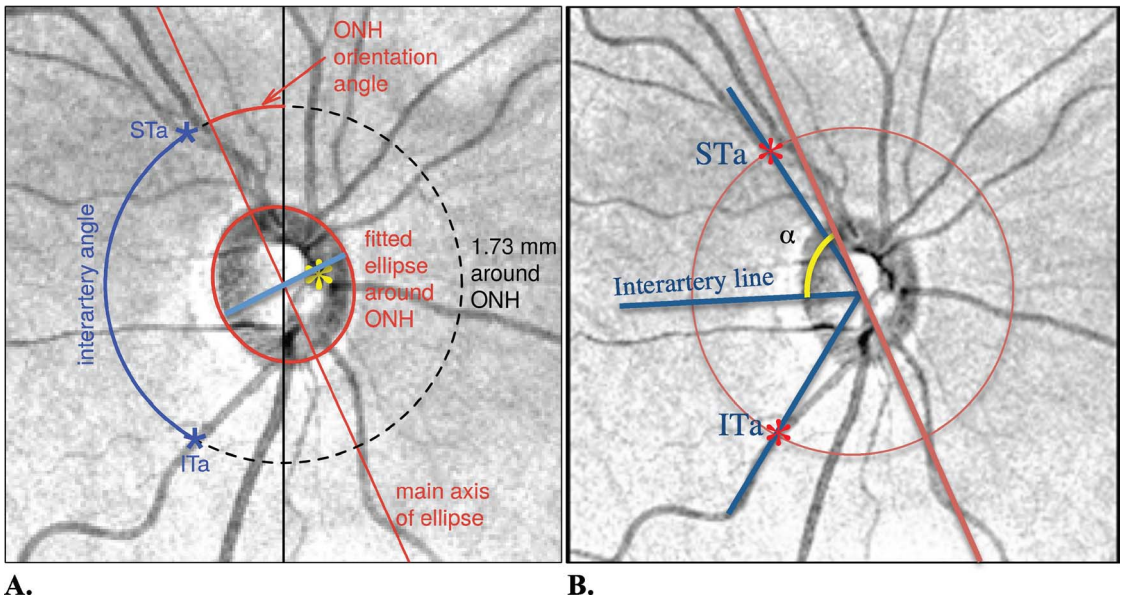

Figure 1. ONH parameters. (A) IAA is the angle between superior temporal artery and inferior temporal artery. ONH orientation angle measures the ROT relative to the vertical reference line. *Yellow asterisk* shows the location of CRVTL. (B) Interartery line divides IAA into two equal superior and inferior temporal sectors. Angle (α) between the main axis of the ellipse and the interartery line measures the degree of ONH TO.

is a rotation measure, which considers individual eye anatomy and determines rotation relative to an anatomical reference related to nerve fiber bundle geometry. A frequently applied reference is the line connecting the fovea to the BMO center (FoBMO axis). Here, we apply an alternative measure, which does not require measurements outside the circumpapillary area: TO was measured as the angle (α) between the main axis of the ellipse and the interartery line, which approximates the center between the two main retinal nerve fiber bundles (Figs. 1B, 2).

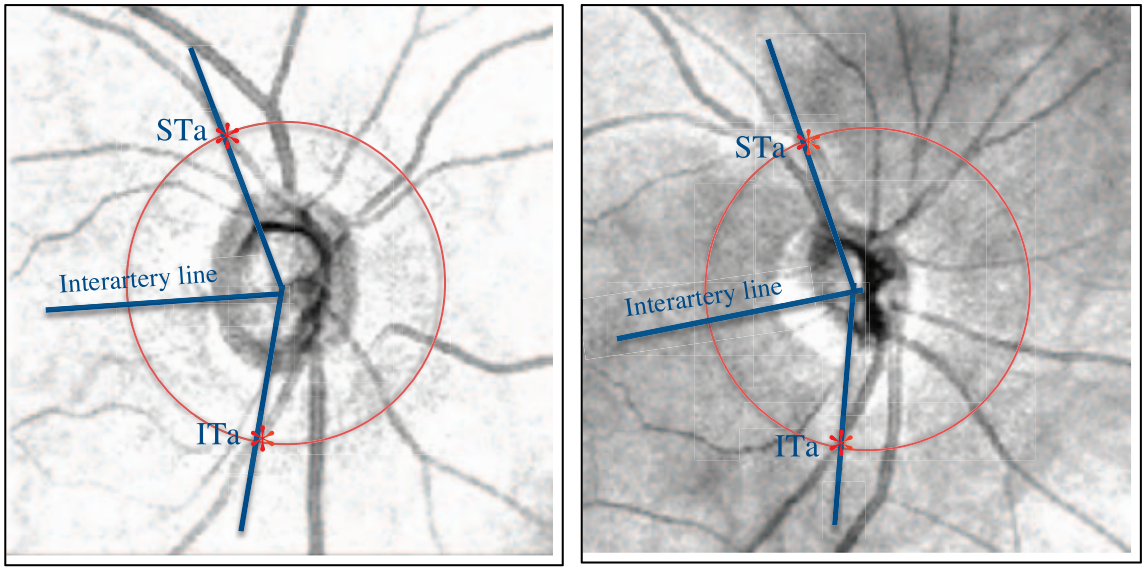

Figure 2. IAA is the angle between superior temporal artery and inferior temporal artery. Interartery line divides IAA into two equal superior and inferior temporal sectors. The angle between interartery line and the horizontal axis of the image frame ranges from −22° to 33° in our study with the median 0.42°. Interartery line is used as an alternative for the line connecting the fovea to the BMO center (FoBMO axis) to measure ONH TO.

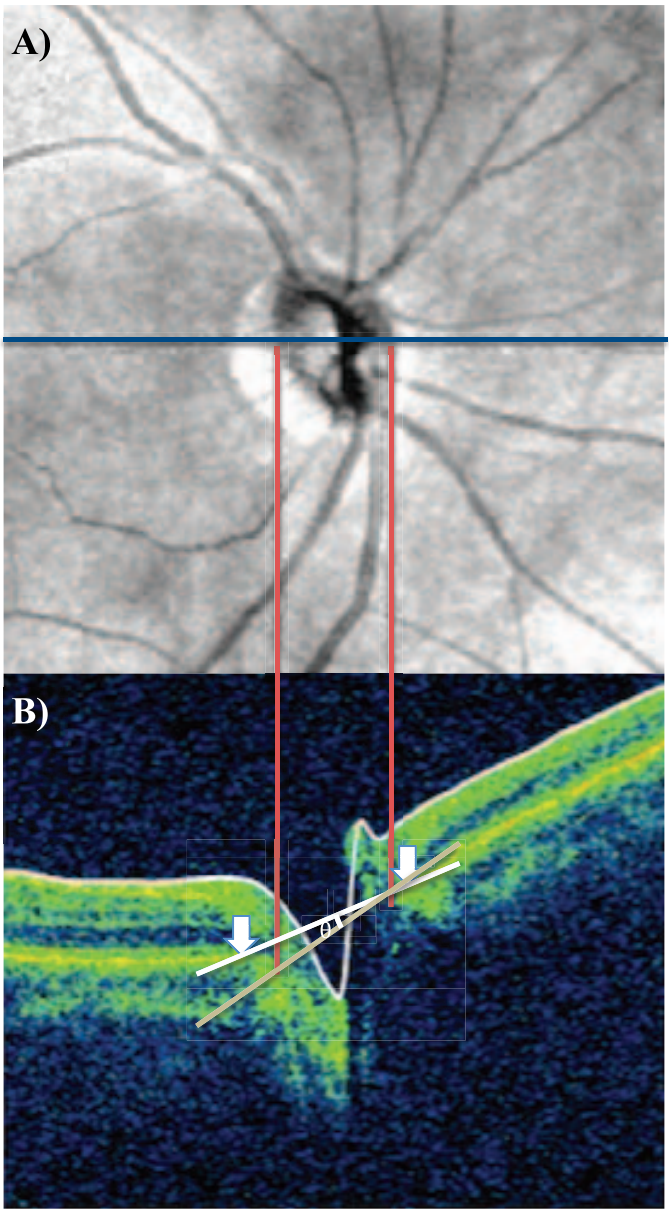

Figure 3. Method used to estimate the vertical ONH tilt angle with Cirrus spectral-domain OCT. (A) The ONH fundus image was used for marking the clinical boundary of ONH on the horizontal axis of the image frame. The *red lines* mark the clinical boundary of the disc and were dropped down to locate the respective points on the OCT horizontal B-scan. (B) The *white arrows* show the inner edges of the BM on each side of the optic nerve head on the horizontal B-scan. The *white line*, connecting the inner edges of the BM, was defined as the reference plane. The *gray line*, connecting the two points marking the clinical disc margin on the OCT image was considered as the ONH plane. The TL (θ) was defined as the angle between the reference plane and the ONH plane.

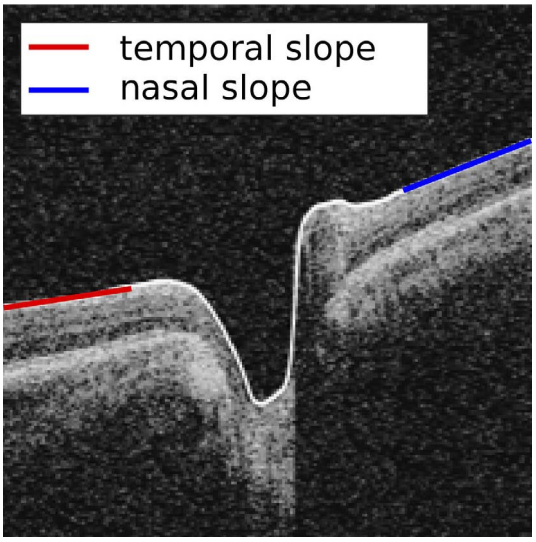

Figure 4. Calculation of retinal ONH CUR on horizontal B-scan. Best lines were fitted to the nasal and temporal inner limiting membrane around ONH on the horizontal B-scan closest to ONH center. CUR was calculated as the mean of the temporal and nasal slopes.

OI was measured as the ratio between the long and the short axis of the optic disc on fundus images. For calculating the vertical ONH tilt (TL) angle, fundus images, and corresponding horizontal B-scans were first aligned. Nasal and temporal clinical boundaries of ONH were marked on the central horizontal axis of the fundus image frames. Vertical lines dropped down on the ONH center horizontal B-scans identified the corresponding anatomical locations to the temporal and nasal clinical disc borders. A line connecting these two points marking the clinical disc margin on the horizontal B-scans was considered as ONH plane. BMO locations were also marked on the horizontal OCT B-scans and the line connecting these points was stated as the reference line. The tilt angle (angle θ) was calculated as the angle between the reference line and ONH plane[13,25] (Fig. 3).

For determining the average curvature of the ONH, we chose the horizontal B-scan closest to the ONH center. On this B-scan, we fitted optimal lines to the inner limiting membrane on the temporal and the nasal edges. Temporal and nasal edges of the B-scan were defined as the areas from the image margins to the points at 50 pixels (25% of the image width) temporal and at 50 pixels nasal to the ONH center, respectively, as denoted by the red and blue lines in Figure 4. Average curvature was defined as the mean of the slopes of the two lines.

Statistical Analysis

We used software R (version 3.1.1; R Foundation) for statistical analysis.

To analyze the impact of ONH related parameters (IAA, OI, ONH rotation, torsion, and tilt, CRVT entry point location, and average curvature) on SE, linear regression was applied, and the resulting regression models were evaluated by two different approaches. The first approach, the likelihood ratio test (LRT), is included because of its widespread use as a comparison with existing studies. The LRT is a null hypothesis significance test (NHST) that compares the likelihood of the respective models with each of the parameters with the null model consisting of the intercept only (no parameter) and calculates a *P* value based on the *F*-test statistic. While this test allows rejecting the null hypothesis in case of *P* less than 0.05, it conceptually fails to provide evidence in favor of the null hypothesis. Moreover, the *P* values do not allow a quantitative comparison between the models based on the different parameters. To address these two issues, as a second approach, a Bayesian model comparison is performed with the Bayes Factor (BF)[26] as a quantitative model selection criterion. Instead of calculating the ratio of maximum likelihood estimates, as performed by LRT, the BF is the quotient of the integral of the likelihoods of the two models (null model versus respective comparison model) over all model parameters. In contrast to *P* values, BFs are quantitative measures to compare the evidence between different models. Following a widely used scale for interpretation of BFs,[26] we consider $3 < BF \leq 20$ as positive, $20 < BF \leq 150$ as strong, and $BF > 150$ as very strong evidence for the alternative over the null hypothesis. Analogously, the reciprocals of these values denote the strength of evidence in favor of the null hypothesis ($1/3 > BF > 1/20$: positive evidence, etc.). For BFs between 1/3 and 3, we cannot favor any of the two models given the data.

By calculating BFs specific to the setting of linear regression[27] for all models consisting of any additive combination of the five parameters compared with the null model and the subsequent model comparison, we not only determine the ONH parameter combination that provides the strongest relationship with SE but also implicitly address the covariance structure of the parameters.

Some researchers[28] have argued that the testing of multiple independent parameters increases the chance of incorrectly rejecting the null hypothesis. As NHST does not allow testing in favor of the null hypothesis, this introduces a systematic error in one testing direction. Therefore, it has been suggested to correct *P* values for multiple comparisons. As LRT is part of NHST, and as our comparison of ONH parameters can be considered a multiple comparison problem, we additionally corrected the LRT *P* values by the Bonferroni method.[28]

Table 1. Demographic Data for the Study Population

N	438
Age: mean [SD], y	59 [13]
Age range (y)	(16–91)
Sex, *n* (%)	
Male	200 (45.7)
Female	238 (54.3)
Race, *n* (%)	
Caucasian	321(73.3)
Asian	32 (7.3)
African American	46 (10.5)
Hispanic	22 (5)
Other	17 (3.9)
Diagnosis	
Glaucoma	208 (47.5)
POAG	150
NTG	18
PXG	14
PDG	15
Other	11
Glaucoma suspect	230 (52.5)
SE: mean [SD], D	−1.18 [2.98]
SE range (D)	(−12.75 to 6.38)
MD: mean [SD], dB	−2.95 [4.18]
MD range (dB)	(−32.04 to 2.01)
PSD: mean [SD], dB	2.89 [2.66]
PSD range (dB)	(0.86–16.13)

Other types of glaucoma include angle closure glaucoma, juvenile, traumatic glaucoma, etc.

Results

A total of 438 eyes of 438 participants were included in this study. Table 1 shows the demographic characteristics of the study population. Our population had an age range of 16 to 91 years with the average of 59 ± 13 years. There was no statistically significant difference for sex in our population (*P* value: 0.069, null hypothesis: 50%). Caucasians formed most of the study population followed by

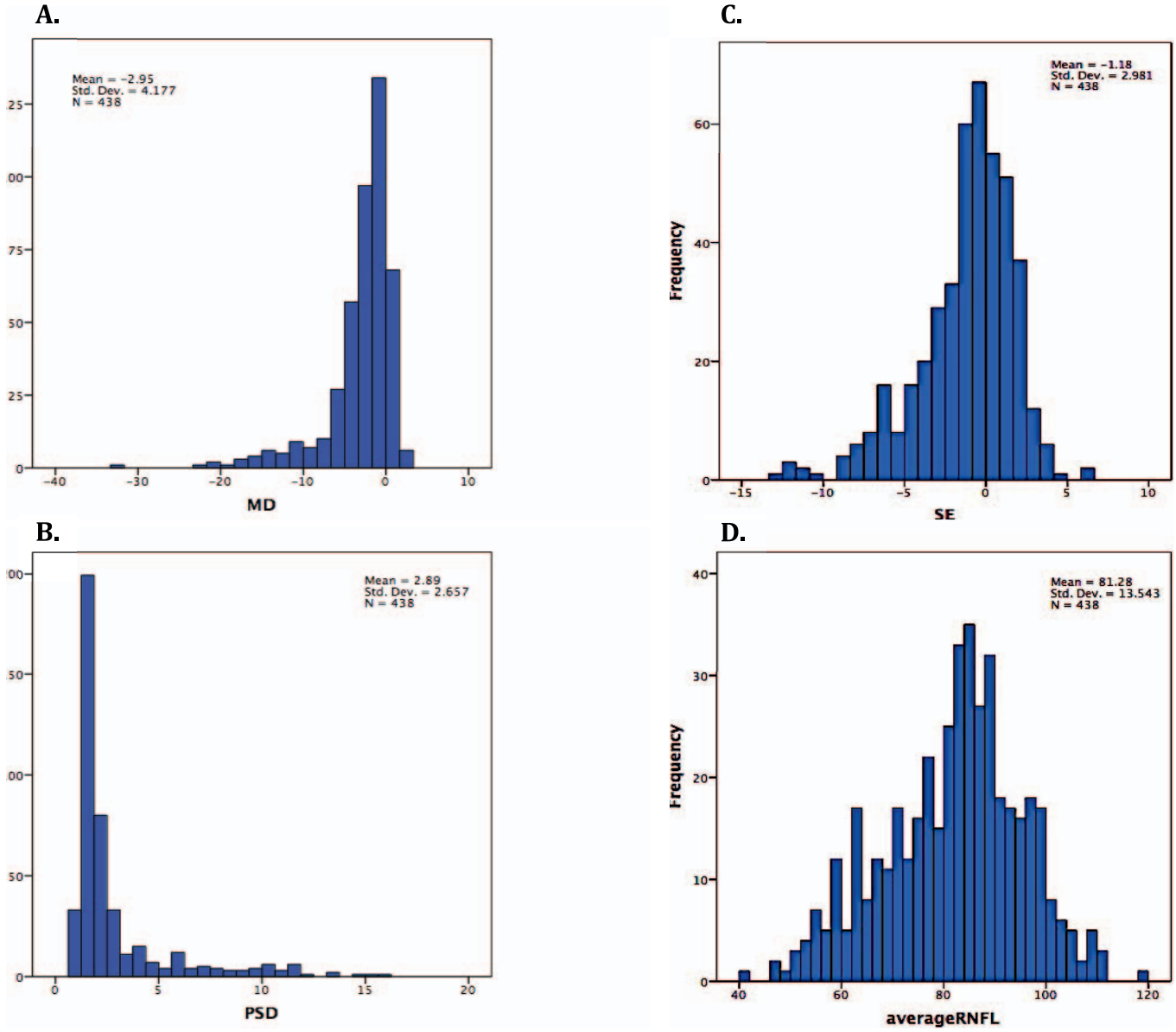

Figure 5. (A–D) Histograms for MD, PSD, SE, and RNFL thickness values in our patient population.

African Americans and Asians. Of the patients, 47.5% (208/438) were diagnosed with glaucoma; 52.5% (230/438) were diagnosed as glaucoma suspect. Our glaucoma population included 150 patients with primary open angle glaucoma (POAG), 18 patients with normal tension glaucoma (NTG), 14 patients with pseudoexfoliation glaucoma (PXG), 15 patients with pigmentary glaucoma (PDG), and 11 patients with other types of glaucoma, such as congenital, juvenile, and so on. The average of glaucoma severity measured by MD was −2.95 ± 4.18 dB with the range of −32 to 2 dB. The average of SE of refractive error was −1.18 ± 2.98 D with the range of −12.75 to 6.38 D (Table 1).

Figures 5A through 5D show the frequency histograms for MD, pattern standard deviation (PSD), SE, and average retinal nerve fiber layer (RNFL) thickness, respectively.

Our results showed that all ONH anatomical parameters except for OI are strongly and independently related to SE, with the strongest relationship for CRVTL followed by ROT, TL, and IAA (BFs: 3.59×10^7, 2645, 1126, and 248, respectively; Table 2). There was no evidence for a relationship between SE and OI or MD (BFs: 0.91 and 0.11, respectively).

Table 2. Linear Regression Models with Spherical Equivalent of Refractive Error as Dependent Variable and Single Optic Nerve Head Parameters as Well as Their Best Combination (According to Bayesian Model Comparison) as Regressors

Model	Regression Equations	Correlation Coefficients (*r*)	LRT *P* Value	Corrected *P* Value	BF
Interartery angle (IAA)	$0.028 \times IAA - 5.30$	0.19	6.48×10^{-5}	4.53×10^{-4}	248
Ovality index (OI)	$4.92 \times OI - 5.73$	0.11	0.035	0.24	0.91
Vertical disc tilt (TL)	$-0.53 \times TL + 3.19$	−0.21	1.27×10^{-5}	8.89×10^{-5}	1126
Disc torsion (TO)	$0.72 \times TO + 72.3$	0.18	1.95×10^{-4}	1.36×10^{-3}	90
Disc rotation (ROT)	$-0.065 \times ROT + 5.80$	−0.22	5.10×10^{-6}	3.57×10^{-5}	2645
Avg. curvature (CUR)	$-3.20 \times CUR - 0.69$	−0.17	4.29×10^{-4}	3.00×10^{-3}	44
CRVT entry point (CRVTL)	$-7.32 \times CRVTL + 3.17$	−0.30	2.25×10^{-10}	1.57×10^{-9}	3.59×10^{7}
Best combination	$0.017 \times IAA + 10.4 \times TL - 0.085 \times TO - 5.83 \times CRVTL - 0.76$		2.20×10^{-16}	N/A	1.25×10^{14}

LRT *P* value: *P* value of likelihood ratio test comparing the model to a null model without parameters (intercept only). Corrected *P* value: LRT *P* value adjusted for multiple comparisons by Bonferroni correction (only for the single parameter models). BF: Bayes factor of the respective model compared with a null model without parameters (intercept only). BF $>$ 3 denotes positive and BF $>$ 20 strong evidence for the respective model over the null model. A table with the complete comparison of all combination models can be found in the Appendix.

For combined factors, ROT and CRVTL had the strongest relationship with SE for two-factor combinations (BF: 3.02×10^{10}). OI, ROT, and CRVTL had the strongest relationship with SE (BF: 3.48×10^{13}) for three-factor combinations. IAA, OI, ROT, and CRVTL had the strongest relationship with SE (BF: 1.25×10^{14}) for four-factor combinations (Table 2). All seven factors together showed strong relationship with SE (BF: 3.50×10^{11}) (Table A in the Appendix).

Table 3 shows correlation coefficients for each parameter and MD. None of the ONH anatomical parameters were significantly correlated to MD.

Table 4 shows model comparisons of linear regression models with and without MD as a parameter. Our results show that glaucoma severity does not explain any additional variance on the associations between each studied anatomical factor and SE (BFs: 0.14–0.18).

To rule out possible specific effects induced by severe glaucoma (MD ≤ -12 dB), we additionally compared severe glaucoma patients with patients with

Table 3. Correlation Coefficients for Each Anatomical Factor as well as Spherical Equivalent Versus Mean Deviation (MD)

Parameter(s)	Correlation Coefficients (r)	*P* Value
SE	−0.02	0.69
IAA	−0.04	0.40
OI	0.06	0.20
TL	0.04	0.38
TO	−0.003	0.96
ROT	0.001	0.98
CUR	0.02	0.64
CRVTL	0.006	0.89

Table 4. Model Comparisons of Linear Regression Models without Versus with Visual Field Mean Deviation (MD) as a Parameter

Model Comparison	LRT *P* Value	BF
IAA vs. IAA+MD	0.80	0.15
OI vs. OI+MD	0.59	0.18
TL vs. TL+MD	0.82	0.15
TO vs. TO+MD	0.69	0.16
ROT vs. ROT+MD	0.68	0.15
CUR vs. CUR+MD	0.74	0.16
CRVTL vs. CRVTL+MD	0.70	0.14

LRT *P* value: *P* value of likelihood ratio test comparing the model with MD to the model without MD. BF: Bayes factor of the respective model with MD compared with the model without MD as parameter. BF $<$ 1/3 denotes positive evidence for the model without MD.

Table 5. Differences between the Means of the Mild and Severe Glaucoma Groups for Each Anatomical Factor

	Mild vs. Severe		Undepressed vs. Severe	
	(MD ≥ -6 dB)	(MD ≤ -12 dB)	(MD ≥ -1 dB)	(MD ≤ -12 dB)
	$n = 377$	$n = 22$	$n = 159$	$n = 22$
Parameter	*t*-test	*P* value	*t*-test	*P* value
IAA	−1.05	0.31	−0.94	0.36
OI	1.38	0.18	1.83	0.08
TL	1.69	0.10	1.58	0.12
TO	−0.43	0.67	−0.52	0.60
ROT	0.32	0.75	0.31	0.76
CUR	0.17	0.86	−0.24	0.81
CRVTL	0.11	0.91	−0.26	0.79

undepressed (MD > -1 dB) or (at most) mild VF loss (MD > -6 dB) for all parameters used in this study. We did not find any significant effect (Table 5).

Discussion

In this study, we investigated the relationships between SE and several anatomical parameters related to the optic nerve head (i.e., IAA, OI, TL, ROT, TO, CRVTL, and CUR), which have relevance for the diagnosis of optic neuropathies like glaucoma, in a population of patients from a large glaucoma clinic. We also studied the impact of glaucoma severity on these relationships. While most previous studies used fundus images and manually traced the border of ONH, we fitted the ONH ellipse automatically using BMO identified on the three-dimensional OCT volume scans for defining the disc border, which promises higher reliability of tilt and torsion definitions. In addition, CRVTL was previously defined on the horizontal axis of ONH[29] while we took disc torsion explicitly into account.

Our results show a strong relationship between SE and six of seven anatomical parameters (Table 2). The strongest relationship was found for CRVTL (BF: 3.59×10^7; more nasal for myopes), followed by ROT (BF: 2645; larger for myopes), TL (BF: 1126; larger for myopes), and IAA (BF: 248; smaller for myopes).

While all ONH parameters have previously been linked to glaucoma,[13,14,19,20,29–34] we did not find any significant correlation between glaucoma severity, measured in the domain of functional vision, with any of the parameters (Table 3). Our findings for TL and MD were in contrast with Hosseini et al.,[25] who demonstrated a statistically significant correlation between vertical optic disc tilt and MD. This lack of significant correlations does not exclude the possibility of interactions between any of the parameters and glaucoma severity. For instance, the relationship between CRVTL and SE might be stronger for severe glaucoma than for mild glaucoma, even though MD alone is not significantly correlated to SE. Therefore, we additionally checked for each parameter if MD explains any variance that was unexplained by the parameter alone. The results of the likelihood ratio tests and the BFs indicate that for none of the parameters MD explains additional variance, which suggests that glaucoma severity does not modulate the relationships between SE and the ONH related parameters (Table 4).

We would like to note that these results do not implicate that these parameters are unrelated to the disease of glaucoma. For instance, previous studies indicate longitudinal shifts of retinal blood vessels with glaucoma severity,[35] and CRVT nasalization might be a result of such glaucoma-related vessel shifts. However, such possible individual longitudinal glaucoma-related changes are too weak to be observed in our cross-sectional statistics and are negligible with respect to the strength of the relationship between SE and each of the parameters, because glaucoma severity does not explain any additional variance. Therefore, SE should be considered a major confounder if these parameters are used to support glaucoma diagnoses, particularly in the absence of patient specific longitudinal measurements.

It has been discussed that scleral changes of myopic eyes during eyeball development are responsible for optic disc morphology including optic disc tilt, torsion, peripapillary atrophy, and consequent increased susceptibility to glaucoma.[13,19,36,37] Previous studies reported that the optic disc is significantly larger and more oval in myopic eyes comparing with

the healthy nonmyopic eyes, and the size and OI of optic disc are correlated with SE[38,39] and AL of the eye.[39] Although the OI is a gold standard for identifying ONH insertion obliqueness in myopic eyes,[23,40] its 2D characteristic does not take original optic disc shape into consideration.[40,41] We did not find evidence for an association between OI and SE (BF: 0.91) in our study and our result was in agreement with Takasaki et al.[40] and Asai et al.[23] who did not find a significant correlation between SE and OI as well. Although OI alone does not result in a satisfying model of SE, it has a strong modulatory effect in combination with other parameters, which is discussed in details further in this section.

We also measured TL using Hosseini et al.[25] method. Our results showed that SE and TL are strongly associated (BF: 1126) and statistically correlated ($r = -0.21$, corrected P value $= 8.89 \times 10^{-5}$), which was in agreement with their study.

Our results showed that SE and ROT are strongly associated (BF = 2645). This was in agreement with previous studies, which reported a higher degree of rotation, especially inferior-temporal rotation in normal and glaucomatous high myopic patients.[13,23,42] Asai et al.[23] did not find significant correlation between ROT and SE ($r = 0.48$, $P = 0.51$) but in contrast to our study, their population was restricted to high myopes only. Park et al.[13,37] found optic disc tilt and rotation as the probable responsible anatomical factors for glaucomatous changes in myopic eyes. They demonstrated that the degree of the vertical ONH tilt and rotation in myopic glaucomatous eyes were highly correlated with the inferior sclera thickness. It is possible that these structural changes, caused by skewed sclera canal shape and thinning of the inferior section of the sclera or lamina cribrosa contribute to glaucomatous findings and corresponding VF defects in highly myopic eyes.[39,43–47]

We also measured TO degree by calculating the angle between the long axis of the ONH and the interartery line that divides the IAA into two equal temporal sectors (superior and inferior). Our results showed a strong association between TO and SE (BF: 90). Chauhan et al.[48] discussed that assessing ONH rotation relative to the fixed vertical or horizontal reference line on OCT images may not be accurate due to the cyclotorsion effect. They showed that the angle of the fovea-BMO axis ranges from 6° to −17° relative to the horizontal axis of the image frame among individuals, which may affect diagnostic accuracy. Our circumpapillary OCT images did not include fovea to allow us to calculate TO angle relative to the fovea-BMO axis. Therefore, we decided to use interartery line as an alternative reference line. Both the fovea-BMO axis and the interartery line equally well address head rotation (cyclotorsion) during the measurement, and both the fovea location relative to the ONH and the major temporal retinal arteries have been shown to be useful as reference coordinates for RNFL thickness measurements[49] (Fig. 2).

Many studies approximate optic disc torsion by rotation without an anatomical reference line (i.e., measured only relative to the vertical reference line of the image plane). We additionally included this reference-free optic disc torsion definition as parameter ROT, mainly for two reasons: First, it allows us to compare our results with these previous studies; second, we can disentangle the effects of the reference line and of the disc rotation. Previous studies found significant correlations between ROT and AL for NTG patients[37,50] as well as between optic disc torsion defined through fovea-BMO axis as reference and AL for healthy myopes.[51] Both results are in agreement with our findings, as we observe strong relationships between SE and both ROT and TO. Unlike previous studies, we are further able to show that the effect of TO on SE is strongly outperformed by the effect of ROT, and the comparison between the combined model (ROT+TO) and ROT alone (Appendix, Table A) suggests that the effect of TO is fully explained by a covariation with ROT and does not explain any additional variance. These results are further supported by the lack of evidence that our reference line (i.e., the interartery line) has any relationship to SE (BF: 0.1, see Appendix, Table A), which indicates that the rotation of the main nerve fiber bundles is independent of ametropia.

To sum up, it is the ROT, independent of the anatomical reference, which is strongly related to ametropia. TO is composed of ROT and an additional parameter, which is independent of ametropia (our anatomical reference line), therefore, the relationship between TO and SE is substantially weaker than between ROT and SE. As noted above, other studies used the fovea-BMO axis as a reference line instead of the interartery line, but previous works did not find significant correlations as well between AL and the fovea-BMO angle in large healthy populations of European[48] and Asian descent.[52] This suggests that our results are generalizable to the alternative torsion definition based on fovea-BMO axis as well.

It has been shown that the angle between the two major RNF bundles, which enter the ONH from temporal direction, linearly decreases with myopia.[14] This finding is of relevance for glaucoma diagnostics as RNFL thickness norms of clinical OCT devices are location-specific, and a natural variation of the nerve fiber bundle location in healthy eyes may result in false-positive glaucoma diagnoses.[24,34,53] As we included the full range of glaucoma severity in our study, and as glaucoma may result in RNFL thinning so that the predisease thickness peaks might become invisible with the progression of the disease, we decided not to determine the RNF bundle angle directly from the RNFL thickness profile. Instead, we exploited the strong correlation of the temporal retinal blood vessels and the predisease RNFL thickness peaks[31,32] and used the IAA as an indirect measure of the RNF bundle angle. Our results showed a strong association between IAA and SE (BF: 248), which is in agreement with the previously reported smaller RNF bundle angle for myopes.[12,42,54,55] Furthermore, studies have shown that the angle between retinal temporal blood vessels decreases over time with progression of myopia.[56]

Our results showed that CRVTL had the strongest relationship as a single anatomical factor with SE (BF: 3.59×10^7). It has been reported that CRVTL shifts nasally during the development of myopia[19] and locates more peripherally in higher myopic eyes.[57] At the same time, CRVTL nasalization has been connected to glaucomatous central vision loss.[29,58] Previous studies[29,57,59,60] discussed that shift of the CRVTL on ONH results in loss of support for the center of lamina cribrosa, decrease in blood supply to the neuroretinal rim distant to the CRVT, and consequent vulnerability to develop glaucoma and central vision scotoma.

Our results also showed that the average CUR is associated with SE (BF: 44). One study reported that oblateness of myopic retinas decreases with an increase in the degree of myopia.[30] An increase in the CUR around ONH changes the OCT measurement angle, which may result in seemingly different RNFLT values for myopic eyes, which, in turn, might impair diagnostic accuracy.

For models with two or more anatomical factors as regressors, our results showed that ROT and CRVTL had the strongest relationship with SE for two-factor combinations (BF: 3.02×10^{10}). This means that including disc rotation into the best model consisting of only one parameter (i.e., CRVTL) increases the evidence by a factor of 841. ROT and CRVTL explain considerably different proportions of the variance of SE. OI, ROT, and CRVTL had the strongest relationship with SE (BF: 3.48×10^{13}) for three-factor combinations. This means that including OI into the best model consisting of two parameters improves the evidence by a factor of 1152. This is particularly noteworthy because OI alone does not result in a satisfying model of SE (BF: 0.91). In other words, while OI in isolation is not useful to model SE, it has a strong modulatory effect in combination with other parameters. A combination of four parameters, IAA, OI, ROT, and CRVTL, had the strongest relationship with SE among all models (BF: 1.25×10^{14}; see Table 2), with an increase in evidence by a factor of 5.7 over the full model including all five parameters. This means, IAA, OI, ROT, and CRVTL explain considerably different proportions of variance, whereas for CUR, correlation effects with the other four parameters outperform possible unexplained variance effects. The explanation of different proportions of variance, and thereby the lack of substantial correlation between IAA, ROT, OI, and CRVTL suggest that each of these four ONH related parameters should be independently considered with respect to confounding effects of SE on the diagnosis of optic neuropathies like glaucoma.

This study has several limitations. Our cross-sectional design cannot determine a causal relationship between ametropia and these anatomical parameters. AL of the eye, which is known to be strongly correlated with SE, is not routinely assessed in clinical practice, and was therefore not available in this study as well. This prevented us from determining if SE changes in our study are indeed the result of axial ametropia rather than lens related effects. However, by excluding cataract patients, we tried to minimize possible nonaxial ametropia effects. Furthermore, our study has validity with respect to clinical settings, as AL is typically not available as well for the diagnosis of optic neuropathies, in contrast to SE. Apart from that, many previous studies defined TO as the angle between the long axis of the ONH ellipse and the line that connects ONH center to the macula. Because our OCT scans did not include macula, we used the interartery line as a reference.

To summarize, we demonstrate that apart from the well-described relationship between ametropia and ocular AL, SE of refractive error is also strongly related to a number of those ONH-related parameters, which have been related to optic neuropathies like glaucoma. This relationship is not modulated by the severity of glaucoma. The present study cannot

address the causality of the reported relationships. Due to the strong correlation between SE and AL, it is likely that variations in eye elongation and shape are responsible for the reported association between SE and several retinal parameters. However, we cannot fully rule out additional contributions of lens effects, and correlations between ONH related parameters have previously been shown with corneal astigmatism (i.e., a clinical phenomenon based in the anterior eye), which causes refractive errors.[61] Our results indicate that refractive error information, which is generally available in a clinical setting, should be considered when interpreting the ONH and its circumpapillary region for diagnostic purposes. Our results have translational relevance as the reported associations between ONH parameters and ametropia may help clinicians to better interpret fundus and OCT images of myopes or hyperopes. Furthermore, they may help OCT manufacturers to adapt their normative data sets by taking additional variables into consideration, such as refractive error or individual RNF bundle locations.

Acknowledgments

Supported by grants from Massachusetts Lions Foundation; Harvard Glaucoma Center of Excellence; Grimshaw-Gudewicz Charitable Foundation; Research to Prevent Blindness; and the National Institutes of Health R01-EY013178.

Disclosure: **N. Baniasadi**, None; **M. Wang**, None; **H. Wang**, None; **M. Mahd**, None; **T. Elze**, None

References

1. Bourne RR, Dineen BP, Ali SM, Noorul Huq DM, Johnson GJ. Prevalence of refractive error in Bangladeshi adults: results of the National Blindness and Low Vision Survey of Bangladesh. *Ophthalmology*. 2004;111:1150–1160.
2. Cheng CY, Hsu WM, Liu JH, Tsai SY, Chou P. Refractive errors in an elderly Chinese population in Taiwan: the Shihpai Eye Study. *Invest Ophthalmol Vis Sci*. 2003;44:4630–4638.
3. Holden BA, Fricke TR, Wilson DA, et al. Global prevalence of myopia and high myopia and temporal trends from 2000 through 2050. *Ophthalmology*. 2016;123:1036–1042.
4. Kempen JH, Mitchell P, Lee KE, et al. The prevalence of refractive errors among adults in the United States, Western Europe, and Australia. *Arch Ophthalmol*. 2004;122:495–505.
5. Wong TY, Foster PJ, Hee J, et al. Prevalence and risk factors for refractive errors in adult Chinese in Singapore. *Invest Ophthalmol Vis Sci*. 2000;41:2486–2494.
6. Saw SM, Katz J, Schein OD, Chew SJ, Chan TK. Epidemiology of myopia. *Epidemiol Rev*. 1996;18:175–187.
7. Jonas JB, Xu L, Wei WB, et al. Myopia in China: a population-based cross-sectional, histological, and experimental study. *Lancet*. 2016;388(suppl 1):S20.
8. Saw SM, Tong L, Chua WH, et al. Incidence and progression of myopia in Singaporean school children. *Invest Ophthalmol Vis Sci*. 2005;46:51–57.
9. Rudnicka AR, Owen CG, Nightingale CM, Cook DG, Whincup PH. Ethnic differences in the prevalence of myopia and ocular biometry in 10- and 11-year-old children: the Child Heart and Health Study in England (CHASE). *Invest Ophthalmol Vis Sci*. 2010;51:6270–6276.
10. Meng W, Butterworth J, Malecaze F, Calvas P. Axial length of myopia: a review of current research. *Ophthalmologica*. 2011;225:127–134.
11. Sowmya V, Venkataramanan VR, Prasad V. Effect of refractive status and axial length on peripapillary retinal nerve fibre layer thickness: an analysis using 3D OCT. *J Clin Diagn Res*. 2015;9:NC01–NC04.
12. Leung CK, Mohamed S, Leung KS, et al. Retinal nerve fiber layer measurements in myopia: an optical coherence tomography study. *Invest Ophthalmol Vis Sci*. 2006;47:5171–5176.
13. Park HY, Choi SI, Choi JA, Park CK. Disc torsion and vertical disc tilt are related to subfoveal scleral thickness in open-angle glaucoma patients with myopia. *Invest Ophthalmol Vis Sci*. 2015;56:4927–4935.
14. Leung CK, Yu M, Weinreb RN, et al. Retinal nerve fiber layer imaging with spectral-domain optical coherence tomography: interpreting the RNFL maps in healthy myopic eyes. *Invest Ophthalmol Vis Sci*. 2012;53:7194–7200.
15. Chang RT, Singh K. Myopia and glaucoma: diagnostic and therapeutic challenges. *Curr Opin Ophthalmol*. 2013;24:96–101.
16. Mitchell P, Hourihan F, Sandbach J, Wang JJ. The relationship between glaucoma and myopia: the Blue Mountains Eye Study. *Ophthalmology*. 1999;106:2010–2015.
17. Mohammad Salih PA. Evaluation of peripapillary retinal nerve fiber layer thickness in myopic

eyes by spectral-domain optical coherence tomography. *J Glaucoma*. 2012;21:41–44.
18. Nakazawa M, Kurotaki J, Ruike H. Longterm findings in peripapillary crescent formation in eyes with mild or moderate myopia. *Acta Ophthalmol*. 2008;86:626–629.
19. Kim TW, Kim M, Weinreb RN, Woo SJ, Park KH, Hwang JM. Optic disc change with incipient myopia of childhood. *Ophthalmology*. 2012;119: 21–26, e21–e23.
20. Samarawickrama C, Mitchell P, Tong L, et al. Myopia-related optic disc and retinal changes in adolescent children from singapore. *Ophthalmology*. 2011;118:2050–2057.
21. Carl Zeiss Meditec Inc. *Cirrus HD-OCT user manual*. Dublin, CA: Carl Zeiss Meditec, Inc.; 2012.
22. Nelder JA, Mead R. A simplex method for function minimization. *Comp J*. 1965;7:308–313.
23. Asai T, Ikuno Y, Akiba M, Kikawa T, Usui S, Nishida K. Analysis of peripapillary geometric characters in high myopia using swept-source optical coherence tomography. *Invest Ophthalmol Vis Sci*. 2016;57:137–144.
24. Hwang YH, Yoo C, Kim YY. Characteristics of peripapillary retinal nerve fiber layer thickness in eyes with myopic optic disc tilt and rotation. *J Glaucoma*. 2012;21:394–400.
25. Hosseini H, Nassiri N, Azarbod P, et al. Measurement of the optic disc vertical tilt angle with spectral-domain optical coherence tomography and influencing factors. *Am J Ophthalmol*. 2013;156:737–744.
26. Kass RE, Raftery AE. Bayes factors. *J Am Stat Assoc*. 1995;90:773–795.
27. Rouder JN, Morey RD. Default bayes factors for model selection in regression. *Multivariate Behav Res*. 2012;47:877–903.
28. Dunn OJ. Multiple comparisons among means. *J Am Stat Assoc*. 1961;56:52–64.
29. Huang H, Jonas JB, Dai Y, et al. Position of the central retinal vessel trunk and pattern of remaining visual field in advanced glaucoma. *Br J Ophthalmol*. 2013;97:96–100.
30. Atchison DA, Pritchard N, Schmid KL, Scott DH, Jones CE, Pope JM. Shape of the retinal surface in emmetropia and myopia. *Invest Ophthalmol Vis Sci*. 2005;46:2698–2707.
31. Hood DC, Fortune B, Arthur SN, et al. Blood vessel contributions to retinal nerve fiber layer thickness profiles measured with optical coherence tomography. *J Glaucoma*. 2008;17:519–528.
32. Hood DC, Salant JA, Arthur SN, Ritch R, Liebmann JM. The location of the inferior and superior temporal blood vessels and interindividual variability of the retinal nerve fiber layer thickness. *J Glaucoma*. 2010;19:158–166.
33. Yamashita T, Asaoka R, Tanaka M, et al. Relationship between position of peak retinal nerve fiber layer thickness and retinal arteries on sectoral retinal nerve fiber layer thickness. *Invest Ophthalmol Vis Sci*. 2013;54:5481–5488.
34. Rho S, Sung Y, Kang T, Kim NR, Kim CY. Improvement of diagnostic performance regarding retinal nerve fiber layer defect using shifting of the normative database according to vessel position. *Invest Ophthalmol Vis Sci*. 2014;55: 5116–5124.
35. Radcliffe NM, Smith SD, Syed ZA, et al. Retinal blood vessel positional shifts and glaucoma progression. *Ophthalmology*. 2014;121:842–848.
36. Ohno-Matsui K, Shimada N, Yasuzumi K, et al. Long-term development of significant visual field defects in highly myopic eyes. *Am J Ophthalmol*. 2011;152:256–265, e251.
37. Park HY, Lee K, Park CK. Optic disc torsion direction predicts the location of glaucomatous damage in normal-tension glaucoma patients with myopia. *Ophthalmology*. 2012;119:1844–1851.
38. Jonas JB, Gusek GC, Naumann GO. Optic disk morphometry in high myopia. *Graefes Arch Clin Exp Ophthalmol*. 1988;226:587–590.
39. Tay E, Seah SK, Chan SP, et al. Optic disk ovality as an index of tilt and its relationship to myopia and perimetry. *Am J Ophthalmol*. 2005; 139:247–252.
40. Takasaki H, Higashide T, Takeda H, Ohkubo S, Sugiyama K. Relationship between optic disc ovality and horizontal disc tilt in normal young subjects. *Jap J Ophthalmol*. 2013;57:34–40.
41. Hyung SM, Kim DM, Hong C, Youn DH. Optic disc of the myopic eye: relationship between refractive errors and morphometric characteristics. *Korean J Ophthalmol*. 1992;6:32–35.
42. Hwang YH, Yoo C, Kim YY. Myopic optic disc tilt and the characteristics of peripapillary retinal nerve fiber layer thickness measured by spectral-domain optical coherence tomography. *J Glaucoma*. 2012;21:260–265.
43. Jonas JB, Berenshtein E, Holbach L. Lamina cribrosa thickness and spatial relationships between intraocular space and cerebrospinal fluid space in highly myopic eyes. *Invest Ophthalmol Vis Sci*. 2004;45:2660–2665.
44. Lee KM, Lee EJ, Kim TW. Lamina cribrosa configuration in tilted optic discs with different tilt axes: a new hypothesis regarding optic disc tilt

and torsion. *Invest Ophthalmol Vis Sci*. 2015;56: 2958–2967.
45. Doshi A, Kreidl KO, Lombardi L, Sakamoto DK, Singh K. Nonprogressive glaucomatous cupping and visual field abnormalities in young Chinese males. *Ophthalmology*. 2007;114:472–479.
46. Vongphanit J, Mitchell P, Wang JJ. Population prevalence of tilted optic disks and the relationship of this sign to refractive error. *Am J Ophthalmol*. 2002;133:679–685.
47. Kim NR, Lim H, Kim JH, Rho SS, Seong GJ, Kim CY. Factors associated with false positives in retinal nerve fiber layer color codes from spectral-domain optical coherence tomography. *Ophthalmology*. 2011;118:1774–1781.
48. Chauhan BC, Danthurebandara VM, Sharpe GP, et al. Bruch's membrane opening minimum rim width and retinal nerve fiber layer thickness in a normal white population: a multicenter study. *Ophthalmology*. 2015;122:1786–1794.
49. Fujino Y, Yamashita T, Murata H, Asaoka R. Adjusting circumpapillary retinal nerve fiber layer profile using retinal artery position improves the structure-function relationship in glaucoma. *Invest Ophthalmol Vis Sci*. 2016;57: 3152–3158.
50. Park HY, Lee KI, Lee K, Shin HY, Park CK. Torsion of the optic nerve head is a prominent feature of normal-tension glaucoma. *Invest Ophthalmol Vis Sci*. 2014;56:156–163.
51. Sung MS, Kang YS, Heo H, Park SW. Characteristics of optic disc rotation in myopic eyes. *Ophthalmology*. 2016;123:400–407.
52. Jonas RA, Wang YX, Yang H, et al. Optic disc - fovea angle: the Beijing Eye Study 2011. *PLoS One*. 2015;10:e0141771.
53. Yoo YC, Lee CM, Park JH. Changes in peripapillary retinal nerve fiber layer distribution by axial length. *Optom Vis Sci*. 2012;89:4–11.
54. Choi SW, Lee SJ. Thickness changes in the fovea and peripapillary retinal nerve fiber layer depend on the degree of myopia. *Korean J Ophthalmol*. 2006;20:215–219.
55. Kang SH, Hong SW, Im SK, Lee SH, Ahn MD. Effect of myopia on the thickness of the retinal nerve fiber layer measured by Cirrus HD optical coherence tomography. *Invest Ophthalmol Vis Sci*. 2010;51:4075–4083.
56. Fledelius HC, Goldschmidt E. Optic disc appearance and retinal temporal vessel arcade geometry in high myopia, as based on follow-up data over 38 years. *Acta Ophthalmol*. 2010;88:514–520.
57. Oh BL, Lee EJ, Kim H, Girard MJ, Mari JM, Kim TW. Anterior lamina cribrosa surface depth in open-angle glaucoma: relationship with the position of the central retinal vessel trunk. *PLoS One*. 2016;11:e0158443.
58. Wang M, Wang H, Pasquale LR, et al. Relationship between central retinal vessel trunk location and visual field loss in glaucoma. *Am J Ophthalmol*. 2017;176:53–60.
59. Jonas JB, Budde WM, Nemeth J, Grundler AE, Mistlberger A, Hayler JK. Central retinal vessel trunk exit and location of glaucomatous parapapillary atrophy in glaucoma. *Ophthalmology*. 2001;108:1059–1064.
60. Jonas JB, Fernandez MC. Shape of the neuroretinal rim and position of the central retinal vessels in glaucoma. *Br J Ophthalmol*. 1994;78: 99–102.
61. Jonas JB, Kling F, Grundler AE. Optic disc shape, corneal astigmatism, and amblyopia. *Ophthalmology*. 1997;104:1934–1937.